



**HAL**  
open science

## Preservation of the isotope signatures in chondritic IOM during aqueous alteration

B. Laurent, L. Remusat, J.-C. Viennet, R. Brunetto, L. Binet, M. Holin, M.  
Ciocco, C. Bouvier, A. Brunelle, S. Bernard

### ► To cite this version:

B. Laurent, L. Remusat, J.-C. Viennet, R. Brunetto, L. Binet, et al.. Preservation of the isotope signatures in chondritic IOM during aqueous alteration. *Geochemical Perspectives Letters*, 2022, 23, pp.28 - 32. 10.7185/geochemlet.2233 . hal-03794414

**HAL Id: hal-03794414**

**<https://hal.science/hal-03794414>**

Submitted on 3 Oct 2022

**HAL** is a multi-disciplinary open access archive for the deposit and dissemination of scientific research documents, whether they are published or not. The documents may come from teaching and research institutions in France or abroad, or from public or private research centers.

L'archive ouverte pluridisciplinaire **HAL**, est destinée au dépôt et à la diffusion de documents scientifiques de niveau recherche, publiés ou non, émanant des établissements d'enseignement et de recherche français ou étrangers, des laboratoires publics ou privés.

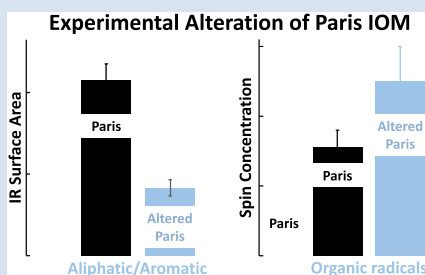
## ■ Preservation of the isotope signatures in chondritic IOM during aqueous alteration

B. Laurent<sup>1\*</sup>, L. Remusat<sup>1</sup>, J.-C. Viennet<sup>1</sup>, R. Brunetto<sup>2</sup>, L. Binet<sup>3</sup>, M. Holin<sup>1</sup>, M. Ciocco<sup>1</sup>,  
C. Bouvier<sup>4</sup>, A. Brunelle<sup>4</sup>, S. Bernard<sup>1</sup>



<https://doi.org/10.7185/geochemlet.2233>

### Abstract



Mighei-type carbonaceous chondrites (CM) figure among the most primitive objects in the solar system. Yet, they all have experienced various degrees of aqueous alteration having modified their insoluble organic matter (IOM), in a sequence that remains to be accurately constrained. Here, we exposed the IOM of Paris, the least altered CM available, to hydrothermal conditions at 150 °C for 49 days and compared the experimental residue to the IOM of two altered CMs likely originating from the same parent body as Paris, namely Aguas Zarcas and Mukundpura. The experimental residue shows a chemical and isotopic composition similar to those of Aguas Zarcas and Mukundpura IOMs, confirming that these CMs can be seen as altered counterparts of Paris. The abundance of organic radicals also increases significantly during the experiment. Isotopic hotspots do not seem to have been lost

during the experiment, suggesting that the hotspots generally observed within the CM IOMs may date back from pre-accretion era. Of note, the Raman signature of the residue differs from that of the CM IOMs, highlighting the need for further experiments better mimicking asteroidal-like conditions.

Received 23 May 2022 | Accepted 26 August 2022 | Published 30 September 2022

### Letter

Carbonaceous chondrites are likely fragments of C-complex asteroids (Vernazza *et al.*, 2017), containing a significant amount of organic matter which may have contributed to the organic inventory of the early Earth. Representing 25 % of the carbonaceous chondrites collected so far (Gounelle *et al.*, 2005), the CMs are among the most primitive objects in the solar system at our disposition. Yet all CMs have experienced various degrees of aqueous alteration, as evidenced by the presence of numerous secondary minerals (Brearley, 2006; Le Guillou *et al.*, 2012; Howard *et al.*, 2015), yielding both weakly altered objects, such as Paris (Hewins *et al.*, 2014) or Asuka (A)-12236 (Glavin *et al.*, 2020), and moderately to totally altered objects in which primary phases have all been replaced. Therefore, a deeper knowledge of the effect of aqueous alteration processes is essential to build a reliable vision of the nature of the primordial, unaltered organic reservoir of CMs.

The CMs exhibit the highest organic carbon contents of all chondrites, with values ranging from 1.5 to 3.4 wt. % (Vacher *et al.*, 2020). Most of this organic component consists of an insoluble organic matter (IOM); macromolecules with rather small aromatic units showing a high degree of crosslinking (Derenne and Robert, 2010; Orthous-Daunay *et al.*, 2013). Of note, the IOM of the most altered CMs are chemically different from

those of the least altered CMs known so far (*i.e.* Paris and Asuka (A)-12236; see Vinogradoff *et al.*, 2017; Glavin *et al.*, 2020). This suggests that the IOM could serve as a chemical tracer of aqueous alteration, and that its early nature can eventually be reconstructed.

Laboratory experiments constitute the most appropriate way to properly constrain the evolution of chondritic IOM during fluid circulation in the asteroidal stage. IOM has been previously shown to experience aromatisation if submitted to high temperature (Okumura and Mimura, 2011; Remusat *et al.*, 2019), as well as significant deuterium depletion (Yabuta *et al.*, 2007; Oba and Naraoka, 2009; Foustoukos *et al.*, 2021), with final D/H values depending on that of the fluid if present. This evolution is significant above 300 °C (Oba and Naraoka, 2009), although the temperature dependence remains limited between 250 and 450 °C (Foustoukos *et al.*, 2021). While these high temperatures certainly reconcile laboratory limitations and astrophysical processes by potentially simulating very slow processes using short duration experiments, they are well beyond the peak temperature undergone by CMs. Although some authors concluded that carbonates were formed at temperature as high as 350 °C, the peak temperature undergone by CMs may not be that far above 100 °C (Guo and Eiler, 2007; Verdier-Paoletti *et al.*, 2017). In that context, we subjected the IOM isolated from the weakly altered Paris (CM2.7) to hydrothermal conditions (150 °C in the

1. Muséum National d'Histoire Naturelle, Sorbonne Université, UMR CNRS 7590, Institut de minéralogie, de physique des matériaux et de cosmochimie, Paris, France
2. Institut d'Astrophysique Spatiale, Université Paris-Saclay, CNRS, 91405, Orsay, France
3. Chimie-ParisTech, PSL University, CNRS, Institut de Recherche de Chimie-Paris (IRCP), Paris, France
4. Sorbonne Université, CNRS, Laboratoire d'Archéologie Structurale et Moléculaire (LAMS – UMR 8220), F-75005, Paris, France

\* Corresponding author (email: [boris.laurent@mnhn.fr](mailto:boris.laurent@mnhn.fr))



presence of liquid water) for 49 days and compared the experimental residue (hereafter referred to as ‘experimentally altered Paris’) to IOM of newly recovered and extensively altered CMs, namely Aguas Zarcas (CM2.2; [Martin and Lee, 2020](#)) and Mukundpura (CM2.0; [Rudraswami et al., 2019](#)). Alteration indices for CMs follows classification from [Rubin et al. \(2007\)](#) based on chemistry and mineralogical evidence, with subtypes defined from totally altered (2.0) to not altered (3.0). The molecular structure of the experimental residue was analysed using X-ray absorption near edge structure (XANES) spectroscopy, Fourier transform infrared (FTIR) spectroscopy and time-of-flight secondary ion mass spectrometry (ToF-SIMS). The radicals in the IOM structure were detected through electron paramagnetic resonance (EPR). The distribution of D- and  $^{15}\text{N}$ -rich hotspots was imaged by NanoSIMS. The limited amount of recovered IOM only allowed elemental ratios determination via NanoSIMS imaging method for the residue ([Remusat et al., 2019](#)). Finally, the degree of carbon organisation was probed using Raman microspectroscopy.

The elemental composition of the Paris IOM experienced modifications during the experiment. Although the S/C value of the residue is not that different from that of the starting material, its N/C value is lower (by about 15 %) and its O/C value is significantly lower (by about 30 %) as indicated by NanoSIMS ([Fig. S-1](#)). The stability at elevated temperature of S-rich groups in IOM was previously established ([Oba and Naraoka, 2009](#); [Okumura and Mimura, 2011](#)). From the XANES spectra, normalised to the total carbon atoms probed, all IOM here are dominated by aromatic groups and contain various amounts of carbonyl, carboxylic and aliphatic carbons ([Fig. 1a](#)). The widening of the aromatic peak towards 285.5 eV observed in the spectrum of the experimental residue indicates the presence of conjugated rings ([Bernard et al., 2010](#)), evidencing ongoing graphitisation. The experimental residue seemingly contains as low oxygen as the IOM of Aguas Zarcas and Mukundpura ([Fig. 1a](#)).

These results are confirmed by infrared spectroscopy ([Fig. 1b,c](#); IR spectra are reported in [Fig. S-2](#)). The experimental residue contains about as many carbonyl groups as the Aguas Zarcas and Mukundpura IOM, *i.e.* significantly fewer than the

Paris IOM ([Fig. 1b,c](#)). Its aliphatic content is low compared to Paris IOM, but higher than in the Aguas Zarcas and Mukundpura IOM. Yet, the  $\text{CH}_2/\text{CH}_3$  of the residue is only slightly lower than that of the Paris IOM, while Aguas Zarcas and Mukundpura IOM have the lower values. The increase of aromaticity during the experiment is also confirmed by TOF-SIMS, with a relatively higher concentration of aromatic cycles in the residue compared to that of the Paris IOM ([Fig. S-3b](#)). Altogether, these spectroscopy and mass spectrometry investigations illustrate that, when exposed to hydrothermal conditions, Paris IOM chemically evolves towards the Aguas Zarcas and Mukundpura. The EPR spectra of the IOMs and of the experimental residue also provide information on the concentration of radicals ([Fig. 2a](#)). Concomitantly to the increase of aromaticity, the abundance of radicals detected increases significantly during the experiment, with a 1.6 times higher content in the experimental residue than in the Paris IOM near room temperature ([Fig. 2b](#)). The concentration of radicals in the experimental residue is systematically higher than in the Aguas Zarcas and Mukundpura IOM, Aguas Zarcas having the lowest abundance.

The IOM of the CM here show identical bulk hydrogen isotopic compositions within error bars ([Fig. 3b](#) for  $\delta\text{D}$  values of  $773 \pm 56$  ‰ for Paris,  $836 \pm 116$  ‰ for Aguas Zarcas and  $780 \pm 91$  ‰ for Mukundpura). The experimental residue is slightly smaller but remains similar within error bars ( $\delta\text{D} = 640 \pm 105$  ‰), and consistent with experimental study on IOM analogues ([Kebukawa et al., 2021](#)). D-rich hotspots usually observed in IOM of CMs ([Busemann et al., 2006](#); [Remusat et al., 2009](#)) are still observed after the experiment ([Fig. 3a](#)), with a distribution of  $\delta\text{D}$  values closer to that of Aguas Zarcas and Mukundpura than to that of Paris, as exemplified by  $\delta\text{D}$  values ranging from 2800 and 3600 ‰ ([Fig. 3a](#)). This effect does not arise from the hotspot distribution, which show only little modification ([Fig. 3c,d](#)). Nevertheless, the present results differ from results of pyrolysis experiments having evidenced that D-rich hotspots could not withstand high temperature ([Remusat et al., 2009, 2019](#)). If hotspots are unaffected by fluid interactions at 150 °C, then their measured isotopic compositions may reasonably correspond to pre-accretion composition of organic grains exposed to various conditions in the protosolar nebula ([Remusat et al., 2010](#)).

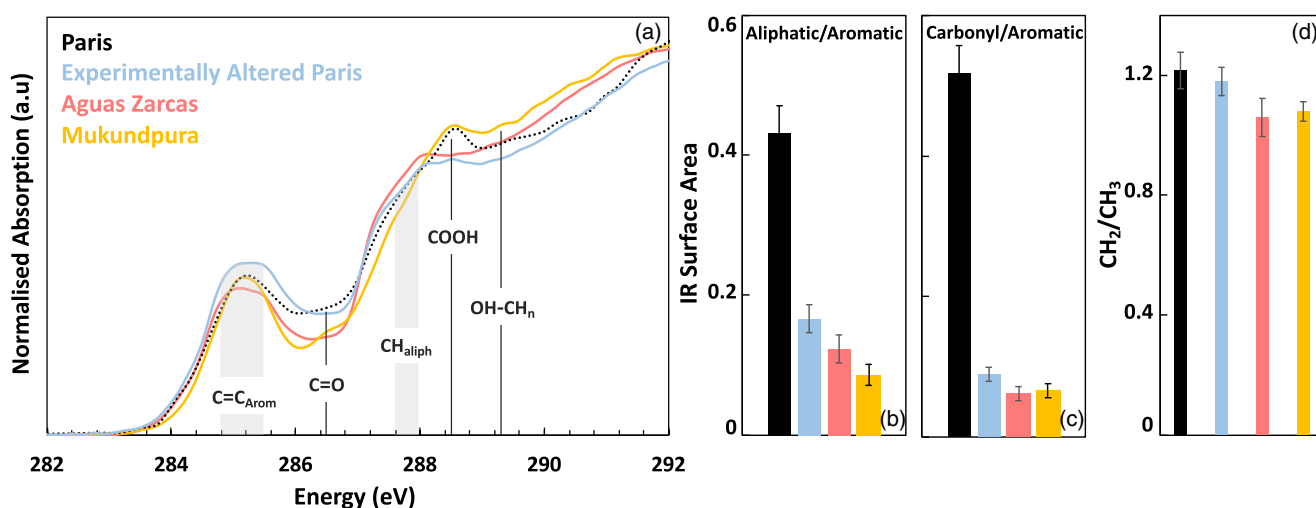


**Figure 1** Spectroscopy investigations. (a) Speciation of organic carbon using near edge X-ray absorption fine structure for Paris (black), the experimentally altered Paris (‘Altered Paris’, blue), and altered CM2 Aguas Zarcas (pink) and Mukundpura (yellow) IOMs. The spectra are dominated by aromatic, carbonyl or carboxylic functional groups, with only a minor contribution of aliphatic groups. (b, c), Relative evolution of infrared surface area for aliphatic and carbonyl bands, relative to aromatic carbon. (d) Intensity ratio for aliphatic  $\text{CH}_2$  ( $2925\text{ cm}^{-1}$ ) and  $\text{CH}_3$  ( $2960\text{ cm}^{-1}$ ) bands.

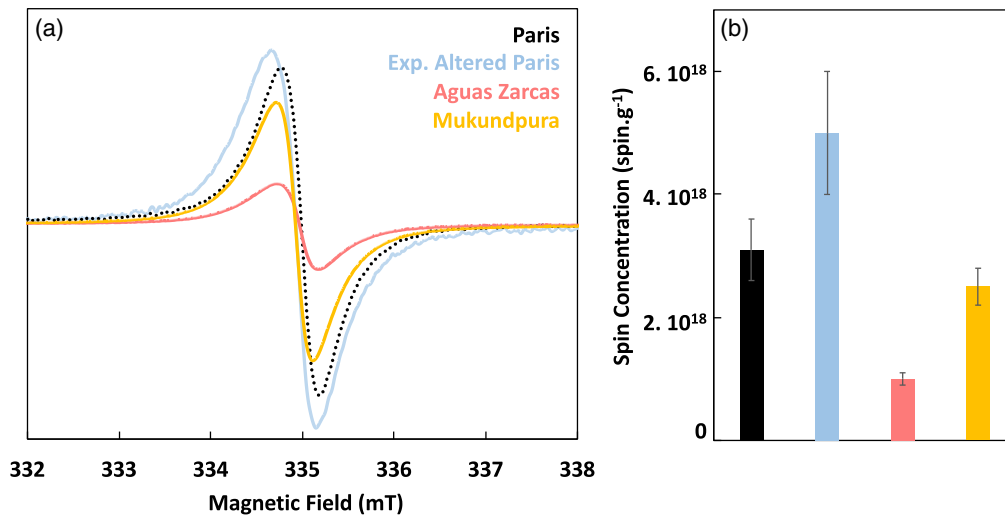


**Figure 2** Detection of organic radicals after experimental alteration. (a) Spectra (microwave absorption derivative) at 280–285 K for experimentally altered Paris (blue), CM2.7 Paris (black) and CM2.2 Aguas Zarcas (red) and CM2.0 Mukundpura (yellow). (b) Concentrations of radicals at 280–285 K.

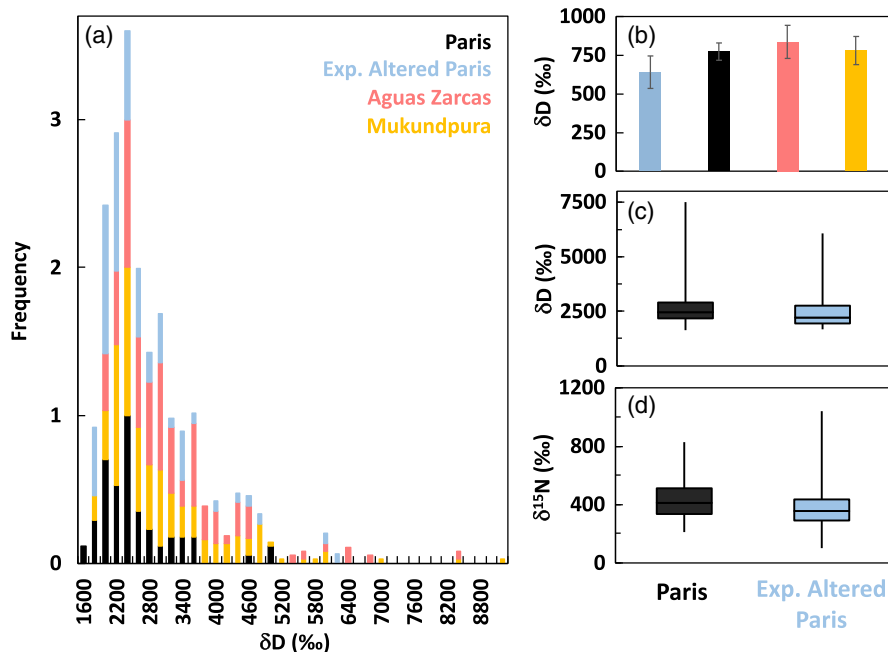


**Figure 3** NanoSIMS investigations. (a) Normalised deuterium-rich hotspot distributions in IOM and bulk hydrogen isotopic compositions of Paris (black), experimentally altered Paris CM2 Aguas Zarcas (pink) and Mukundpura (yellow). Distribution are normalised to the number of occurrences and stacked. (b) The bulk hydrogen isotopic compositions of the different CMs and the experimental residue. (c, d) Evolution of the hotspot signatures for hydrogen (analysed on  $3600 \mu\text{m}^2$  surface) and nitrogen isotopes (analysed on  $2400 \mu\text{m}^2$  surface; images are reported on Fig. S-4).

The Raman spectra of the experimental residue and from the natural objects exhibit two main bands, the so-called defect (D,  $1355 \text{ cm}^{-1}$ ) and graphite (G,  $1595 \text{ cm}^{-1}$ ) bands (Fig. 4a). These two bands are broad for all the samples, and correspond to a highly disordered carbon structure, typical of low thermal alteration (Quirico *et al.*, 2018). All CMs here present similar band widths ( $\text{FWHM}_{\text{D,G}}$ ) and surface area ratios ( $A_{\text{D}}/A_{\text{G}}$ ; Fig. 4b,c). However, the Raman spectrum of the experimental residue is different and rather corresponds to carbonaceous material with an apparent lower degree of carbon organisation, even though it contains more conjugated cycles as indicated by its XANES spectrum.

All considered, the experimental residue is chemically similar to the IOM of CMs having undergone aqueous alteration (Fig. 1). In contrast to the common belief that radicals should be destroyed during alteration, the residue also contains an additional population of radicals easily detected at room temperature (Fig. 2b). Its isotopic composition is not that different from that of the Paris IOM, while its microstructure (*i.e.* its degree of carbon organisation) differs from that of both the Paris, Aguas Zarcas and Mukundpura IOM. Based upon the present results, we suggest that aqueous alteration is not solely responsible for the differences existing between the CM, hence pre-accretion signatures are still detected in natural objects. Nevertheless, we

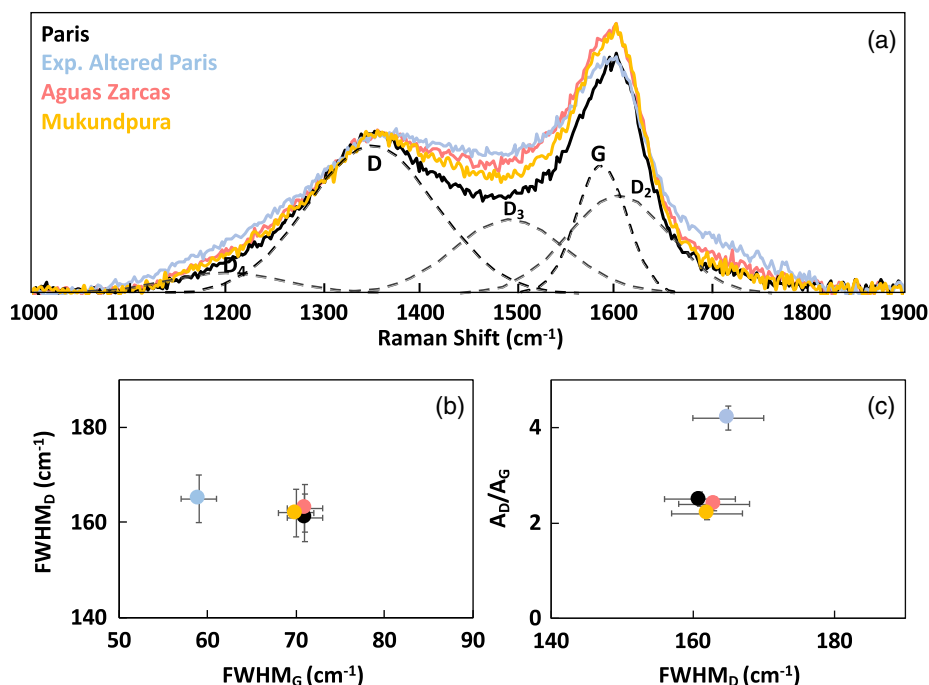


**Figure 4** Structural evolution of Paris IOM under asteroidal conditions. (a) Raman spectra of Paris (black), experimentally altered Paris H<sub>2</sub>O ('Altered Paris', blue), and altered CM2 Aguas Zarcas (pink) and Mukundpura (yellow). Positions of G, D and minor defect bands are also reported. (b) Comparison of Raman D and G band widths for Paris (black), experimentally altered Paris (blue) and altered CM2 Aguas Zarcas (pink) and Mukundpura (yellow). (c) Evolution of band surface area ratio as function D band width for altered Paris, and the natural objects.

cannot exclude that the present experimental conditions do not perfectly mimic those of natural settings. For these experiments to be closer to the conditions existing in the parent body of CMs, additional parameters should have been considered, such as the presence of mineral phases. Clay minerals constitute the main phase of aqueously altered chondrites (Beck *et al.*, 2010) and are closely associated with organic matter in chondrites (Le Guillou *et al.*, 2014). Clay minerals can in fact adsorb, trap and/or store organic molecules (Lagaly *et al.*, 2013), and possibly inhibit the production of IOM under asteroidal conditions (Viennet *et al.*, 2022). A potential key limitation here could be the strict closed system conditions under which the present experiments have been conducted. While it is consistent with the isochemical alteration undergone by primitive chondrites (Bland *et al.*, 2009), the diversity of d<sup>18</sup>O values of the minerals phases comprising CM2s (*e.g.*, Kimura *et al.*, 2020) pleads in favour of a relatively open system. Hence, while showing chemical and isotopic composition congruent with altered chondritic matter, the present study highlights the need for further experiments to better constrain the effect of aqueous alteration on the chemical, isotopic and structural evolution of IOM during asteroidal aqueous alteration and eventually build a reliable vision of the nature of the primordial, unaltered organic reservoir of CMs.

## Acknowledgements

This work was supported by the European Research Council *via* the ERC project HYDROMA (grant agreement No. 819587). The NanoSIMS facility at the Muséum National d'Histoire Naturelle in Paris was established by funds from the CNRS, Région Ile de France, Ministère délégué à l'Enseignement supérieur et à la Recherche, and the Muséum National d'Histoire Naturelle. We thank F. Borondics and C. Sandt for precious help at the SMIS beamline. The FTIR micro-spectroscopy

measurements were supported by grants from Region Ile-de-France (DIM-ACAV) and SOLEIL. Boris Laurent thanks Olivier Beyssac for his technical help and advices. We thank Dionysis Foustoukos and the two anonymous reviewers for their valuable comments, and Francis McCubbin for editorial handling.

Editor: Francis McCubbin

## Additional Information

Supplementary Information accompanies this letter at <https://www.geochemicalperspectivesletters.org/article2233>.



© 2022 The Authors. This work is distributed under the Creative Commons Attribution Non-Commercial No-Derivatives 4.0

License, which permits unrestricted distribution provided the original author and source are credited. The material may not be adapted (remixed, transformed or built upon) or used for commercial purposes without written permission from the author. Additional information is available at <https://www.geochemicalperspectivesletters.org/copyright-and-permissions>.

**Cite this letter as:** Laurent, B., Remusat, L., Viennet, J.-C., Brunetto, R., Binet, L., Holin, M., Ciocco, M., Bouvier, C., Brunelle, A., Bernard, S. (2022) Preservation of the isotope signatures in chondritic IOM during aqueous alteration. *Geochem. Persp. Let.* 23, 28–32. <https://doi.org/10.7185/geochemlet.2233>

## References

BERNARD, S., BEYSSAC, O., BENZERARA, K., FINDLING, N., TZVETKOV, G., BROWN JR, G.E. (2010) XANES, Raman and XRD study of anthracene-based cokes and saccharose-based chars submitted to high-temperature pyrolysis. *Carbon* 48, 2506–2516. <https://doi.org/10.1016/j.carbon.2010.03.024>



- BLAND, P.A., JACKSON, M.D., COKER, R.F., COHEN, B.A., WEBBER, J.B.W., LEE, M.R., DUFFY, C.M., CHATER, R.J., ARDAKANI, M.G., MCPHAIL, D.S., MCCOMB, D.W., BENEDEX, G.K. (2009) Why aqueous alteration in asteroids was isochemical: High porosity  $\neq$  high permeability. *Earth and Planetary Science Letters* 287, 559–568. <https://doi.org/10.1016/j.epsl.2009.09.004>
- BECK, P., QUIRICO, E., MONTES-HERNANDEZ, G., BONAL, L., BOLLARD, J., ORTHOUS-DAUNAY, F.R., HOWARD, K.T., SCHMITT, B., BRISSAUD, O., DESCHAMPS, F., WUNDER, B., GUILLLOT, S. (2010) Hydrous mineralogy of CM and CI chondrites from infrared spectroscopy and their relationship with low albedo asteroids. *Geochimica et Cosmochimica Acta* 74, 4881–4892. <https://doi.org/10.1016/j.gca.2010.05.020>
- BREARLEY, A.J. (2006) The action of water. *Meteorites and the Early Solar System II* 943, 587–624.
- BUSEMANN, H., YOUNG, A.F., ALEXANDER, C.M.O.D., HOPPE, P., MUKHOPADHYAY, S., NITTLER, L.R. (2006) Interstellar chemistry recorded in organic matter from primitive meteorites. *Science* 312(5774), 727–730. <https://doi.org/10.1126/science.1123878>
- DERENNE, S., ROBERT, F. (2010) Model of molecular structure of the insoluble organic matter isolated from Murchison meteorite. *Meteoritics & Planetary Science* 45, 1461–1475. <https://doi.org/10.1111/j.1945-5100.2010.01122.x>
- FOUSTOUKOS, D.I., ALEXANDER, C.M.O.D., CODY, G.D. (2021) H and N systematics in thermally altered chondritic insoluble organic matter: An experimental study. *Geochimica et Cosmochimica Acta* 300, 44–64. <https://doi.org/10.1016/j.gca.2021.01.021>
- GLAVIN, D.P., MCLAIN, H.L., DWORIN, J.P., PARKER, E.T., ELSLA, J.E., APONTE, J.C., SIMKUS, D.N., POZARYCHI, C.I., GRAHAM, H.V., NITTLER, L., ALEXANDER, C.M.O.D. (2020) Abundant extraterrestrial amino acids in the primitive CM carbonaceous chondrite Asuka 12236. *Meteoritics & Planetary Science* 55, 1979–2006. <https://doi.org/10.1111/maps.13560>
- GOUNELLE, M., ENGRAND, C., ALARD, O., BLAND, P.A., ZOLENSKY, M.E., RUSSELL, S.S., DUPRAT, J. (2005) Hydrogen isotopic composition of water from fossil micrometeorites in howardites. *Geochimica et Cosmochimica Acta* 69, 3431–3443. <https://doi.org/10.1016/j.gca.2004.12.021>
- GUO, W., EILER, J.M. (2007) Temperatures of aqueous alteration and evidence for methane generation on the parent bodies of the CM chondrites. *Geochimica et Cosmochimica Acta* 71, 5565–5575. <https://doi.org/10.1016/j.gca.2007.07.029>
- HEWINS, R.H., BOUROT-DENISE, M., ZANDA, B., LEROUX, H., BARRAT, J.A., HUMAYUN, M., GÖPEL, C., GREENWOOD, R.C., FRANCHI, I.A., PONT, S., LORAND, J.P., COURNEDE, C., GATTACCECA, J., ROCHETTE, P., KUGA, M., MARROCCHI, Y., MARTY, B. (2014) The Paris meteorite, the least altered CM chondrite so far. *Geochimica et Cosmochimica Acta* 124, 190–222. <https://doi.org/10.1016/j.gca.2013.09.014>
- HOWARD, K.T., ALEXANDER, C.M.O.D., SCHRADER, D.L., DYL, K.A. (2015) Classification of hydrous meteorites (CR, CM and C2 ungrouped) by phyllosilicate fraction: PSD-XRD modal mineralogy and planetesimal environments. *Geochimica et Cosmochimica Acta* 149, 206–222. <https://doi.org/10.1016/j.gca.2014.10.025>
- KEBUKAWA, Y., KOBAYASHI, S., KAWASAKI, N., WANG, Y., YURIMOTO, H., CODY, G.D. (2021) Hydrogen isotopic exchange kinetics between organic matter and water: Implications for chemical evolution during meteorite parent body processing. *Meteoritics & Planetary Science* 56, 440–454. <https://doi.org/10.1111/maps.13629>
- KIMURA, M., IMAE, N., KOMATSU, M., BARRAT, J.A., GREENWOOD, R.C., YAMAGUCHI, A., NOGUCHI, T. (2020) The most primitive CM chondrites, Asuka 12085, 12169, and 12236, of subtypes 3.0–2.8: Their characteristic features and classification. *Polar Science* 26, 100565. <https://doi.org/10.1016/j.polar.2020.100565>
- LE GUILLOU, C., ROUZAUD, J. N., BONAL, L., QUIRICO, E., DERENNE, S., REMUSAT, L. (2012) High resolution TEM of chondritic carbonaceous matter: Metamorphic evolution and heterogeneity. *Meteoritics & Planetary Science* 47, 345–362. <https://doi.org/10.1111/j.1945-5100.2012.01336.x>
- LE GUILLOU, C., BERNARD, S., BREARLEY, A.J., REMUSAT, L. (2014) Evolution of organic matter in Orgueil, Murchison and Renazzo during parent body aqueous alteration: In situ investigations. *Geochimica et Cosmochimica Acta* 131, 368–392. <https://doi.org/10.1016/j.gca.2013.11.020>
- LAGALY, G., OGAWA, M., DÉKÁNY, I. (2013) Clay mineral–organic interactions. *Developments in Clay Science* 5, 435–505. <https://doi.org/10.1016/B978-0-08-098258-8.00015-8>
- MARTIN, P.M.C., LEE, M.E. (2020) Degree of Aqueous Alteration of the CM Carbonaceous Chondrite Aguas Zarcas: Implications for Understanding Ryugu and Bennu. 51<sup>st</sup> Lunar and Planetary Science Conference, abstract #2326.
- OKUMURA, F., MIMURA, K. (2011) Gradual and stepwise pyrolyses of insoluble organic matter from the Murchison meteorite revealing chemical structure and isotopic distribution. *Geochimica et Cosmochimica Acta* 75, 7063–7080. <https://doi.org/10.1016/j.gca.2011.09.015>
- ORTHOS-DAUNAY, F.R., QUIRICO, E., BECK, P., BRISSAUD, O., DARTOIS, E., PINO, T., SCHMITT, B. (2013) Mid-infrared study of the molecular structure variability of insoluble organic matter from primitive chondrites. *Icarus* 223, 534–543. <https://doi.org/10.1016/j.icarus.2013.01.003>
- QUIRICO, E., BONAL, L., BECK, P., YABUTA, H., NAKAMURA, T., NAKATO, A., FLANDINET, L., MONTAGNAC, G., SCHMITT-KOPPLIN, P., HERD, C.D.K. (2018) Prevalence and nature of heating processes in CM and C2-ungrouped chondrites as revealed by insoluble organic matter. *Geochimica et Cosmochimica Acta* 241, 17–37. <https://doi.org/10.1016/j.gca.2018.08.029>
- REMUSAT, L., ROBERT, F., MEIBOM, A., MOSTEFAOULI, S., DELPOUX, O., BINET, L., GOURIER, D., DERENNE, S. (2009) Proto-planetary disk chemistry recorded by D-rich organic radicals in carbonaceous chondrites. *The Astrophysical Journal* 698, 2087. <https://doi.org/10.1088/0004-637X/698/2/2087>
- REMUSAT, L., GUAN, Y., WANG, Y., EILER, J.M. (2010) Accretion and preservation of D-rich organic particles in carbonaceous chondrites: Evidence for important transport in the early solar system nebula. *The Astrophysical Journal* 713 (2), 1048. <https://doi.org/10.1088/0004-637X/713/2/1048>
- REMUSAT, L., BONNET, J.Y., BERNARD, S., BUCH, A., QUIRICO, E. (2019) Molecular and isotopic behavior of insoluble organic matter of the Orgueil meteorite upon heating. *Geochimica et Cosmochimica Acta* 263, 235–247. <https://doi.org/10.1016/j.gca.2019.07.013>
- RUBIN, A.E., TRIGO-RODRÍGUEZ, J.M., HUBER, H., WASSON, J.T. (2007) Progressive aqueous alteration of CM carbonaceous chondrites. *Geochimica et Cosmochimica Acta* 71, 9, 2361–2382. <https://doi.org/10.1016/j.gca.2007.02.008>
- RUDRASWAMI, N.G., NAIK, A.K., TRIPATHI, R.P., BHANDARI, N., KARAPURKAR, S.G., PRASAD, M. S., BABU, E.V.S.S.K., SARATHI, U.V. (2019) Chemical, isotopic and amino acid composition of Mukundpura CM2.0 (CM1) chondrite: Evidence of parent body aqueous alteration. *Geoscience Frontiers* 10, 495–504. <https://doi.org/10.1016/j.gsf.2018.02.001>
- VACHER, L.G., PIANI, L., RIGAUDIER, T., THOMASSIN, D., FLORIN, G., PIRALLA, M., MARROCCHI, Y. (2020) Hydrogen in chondrites: Influence of parent body alteration and atmospheric contamination on primordial components. *Geochimica et Cosmochimica Acta* 281, 53–66. <https://doi.org/10.1016/j.gca.2020.05.007>
- VERDIER-PAOLETTI, M. J., MARROCCHI, Y., AVICE, G., ROSKOSZ, M., GURENKO, A., GOUNELLE, M. (2017) Oxygen isotope constraints on the alteration temperatures of CM chondrites. *Earth and Planetary Science Letters* 458, 273–281. <https://doi.org/10.1016/j.epsl.2016.10.055>
- VERNAZZA, P., CASTILLO-ROGEZ, J., BECK, P., EMERY, J., BRUNETTO, R., DELBO, M., MARSSSET, M., MARCHIS, F., GROUSSIN, O., ZANDA, B., LAMY, P., MOUSIS, O., DELSANTI, A., DJOUADI, Z., DIONNET, Z., BORONDICS, F., CARRY, B. (2017) Different origins or different evolutions? Decoding the spectral diversity among C-type asteroids. *The Astronomical Journal* 153, 72. <https://doi.org/10.3847/1538-3881/153/2/72>
- VIENNET, J.C., LE GUILLOU, C., REMUSAT, L., BARON, F., DELBES, L., BLANCHENET, A.M., LAURENT, B., CRIQUET, I., BERNARD, S. (2022) Experimental investigation of Fe-clay/organic interactions under asteroidal conditions. *Geochimica et Cosmochimica Acta* 318, 352–365. <https://doi.org/10.1016/j.gca.2021.12.002>
- VINOGRADOFF, V., LE GUILLOU, C., BERNARD, S., BINET, L., CARTIGNY, P., BREARLEY, A.J., REMUSAT, L. (2017) Paris vs. Murchison: Impact of hydrothermal alteration on organic matter in CM chondrites. *Geochimica et Cosmochimica Acta* 212, 234–252. <https://doi.org/10.1016/j.gca.2017.06.009>
- YABUTA, H., WILLIAMS, L.B., CODY, G.D., ALEXANDER, C.M.O.D., PIZZARELLO, S. (2007) The insoluble carbonaceous material of CM chondrites: A possible source of discrete organic compounds under hydrothermal conditions. *Meteoritics & Planetary Science* 42, 37–48. <https://doi.org/10.1111/j.1945-5100.2007.tb00216.x>



# Preservation of the isotope signatures in chondritic IOM during aqueous alteration

B. Laurent, L. Remusat, J.-C. Viennet, R. Brunetto, L. Binet, M. Holin, M. Ciocco, A. Brunelle, C. Bouvier, S. Bernard

## Supplementary Information

The Supplementary Information includes:

- Sample Selection
- Experimental Procedure
- XANES Spectroscopy
- Raman Spectroscopy
- Infrared Spectroscopy
- TOF SIMS Mass Spectrometry
- Elemental Analysis
- NanoSIMS Mass Spectrometry
- EPR Spectroscopy
- Figures S-1 to S-4
- Table S-1
- Supplementary Information References

## Sample Selection

The IOM of all chondrites were isolated by HF/HCl treatments as described in Vinogradoff *et al.* (2017) for Paris. Samples of Aguas Zarcas (Alajuela province, Costa Rica, 2019) and Mukundpura (Rajasthan, India, 2017) were provided by Luc Labenne. Initially, 4.4 and 6.3 g of bulk material were respectively separated and crushed using a stainless-steel mortar. The soluble fraction was isolated using successive extraction in

solvents, in Teflon vials, partly immersed in a sonicated H<sub>2</sub>O bath. The extraction was performed using the protocol described in the Supplementary Information of Laurent *et al.* (2022).

## Experimental Procedure

A starting mixture of 10 µL ultrapure water (produced by a Veolia Chorus 3 system, resistivity 18.2 MΩ and COT <3 ppb) and 10 µg of Paris IOM was loaded in pure gold capsule. The capsule was closed by arc welding, using Lampert pulse welder, set a 28mV and 5ms pulse, and loaded into a 23 mL PTFE reactor. The reactor was filled with 12 mL of the same ultrapure water, in order to work at conditions of water vapour saturation pressure ( $P_{\text{sat}} = 6$  bars). The reactor was then put in an oven with temperature accurately regulated at 150 °C for 49 days. At the end of the experiment, the reactor was allowed to cool down freely. Capsule integrity afterwards was checked using optical microscope. The capsule was intact, and the solid residue was recovered by centrifugation, washed successively with ultrapure water, high grade ethanol, dichloromethane, and then air dried.

## XANES Spectroscopy

For XANES data collection, the HERMES STXM beamline was operated at the synchrotron SOLEIL (Belkhou *et al.*, 2015; Swaraj *et al.*, 2017; Hitchcock, 2018). In order to prevent a carbon contamination, all the beamline's optical elements were exposed to a continuous flow of pure O<sub>2</sub>. The 3p Rydberg peak of gaseous CO<sub>2</sub> at 294.96 eV was used for energy calibration. Image stacks were collected over the carbon absorption range (270–350 eV) at every 0.1 eV. The dwell time was set below 1ms, in order to any prevent irradiation damages (Wang *et al.*, 2009). From the method described in Le Guillou *et al.* (2018), the background of XANES spectra was subtracted using a power law, and the integration of the signal from the pre-edge region up to the mean ionisation energy (*e.g.*, 282.0–291.5 eV at the C K edge) allowed the normalisation of each spectrum to the carbon quantity and the quantification of functional group concentrations (Le Guillou *et al.*, 2018).

## Raman Spectroscopy

Raman Spectra were acquired using a Renishaw InVia spectrometer, associated with an argon laser (514.5 nm) for a nominal power of 36 mW. To prevent any laser-induced heating, the laser was used at 0.1 % of its power, yielding a planar resolution of ~ 2 µm for a power of less than 10 µW delivered at the sample surface. For laser power >0.1 %, clear indication of laser-induced heating was observed, with a shift of the G band towards low wavenumbers (Fig. S-4). Data were collected by averaging 500 accumulations on a static range between 500 and 2000 cm<sup>-1</sup>. Linear shaped baseline between 1000 and 1900 cm<sup>-1</sup> was applied, using the Fityk software (Wojdyr 2010). The peak deconvolution utilises 5 Gaussians at fixed position, to measure the evolution of the different defect bandwidths in regard to the hydrothermal alteration. Main G and D bands were set at 1595 and 1355 cm<sup>-1</sup>, and the minor defect bands named D<sub>1,2,4</sub> were respectively fixed at 1200, 1500 and 1620 cm<sup>-1</sup>. Standard deviations are given by the covariance value (%) between the spectra and their fit, and calculated from the weighted sum squared residual (WSSR).



## Infrared Spectroscopy

Infrared spectra were collected on IOM samples deposited on IR transparent CaF<sub>2</sub> windows at the SMIS beamline of the SOLEIL synchrotron (France) using an Agilent Cary 670/620 micro-spectrometer equipped with a 128x128 pixel Focal Plane Array detector (3900–800 cm<sup>-1</sup>) and with a single point MCT detector (6000–650 cm<sup>-1</sup>). MCT detector was used and the internal globar source at 4 cm<sup>-1</sup> spectral resolution. The micro-IR spectra were acquired in transmittance geometry (256 accumulated scans per sample), with respect to clean CaF<sub>2</sub> areas, using a x25 objective and 80 μm spot size on the focal plane. Measurements were performed using KBr pellets. Using Fityk software, IR spectra were baseline corrected using a spline functions, with 6 anchor points at 740, 820, 920, 1270, 3600, 4000 cm<sup>-1</sup>. Gaussian fit was applied, at fixed positions (1040, 1245, 1385, 1450, 1590 and 1710 cm<sup>-1</sup>). Aromatic C-H are taken at 1590 cm<sup>-1</sup>, and aliphatic C-C were taken at 1385 and 1450 cm<sup>-1</sup> (mean values reported here), and C-O at 1710 cm<sup>-1</sup>. For the CH<sub>2</sub>/CH<sub>3</sub> determination, additional linear fit was applied between 2700 and 3100 cm<sup>-1</sup>, and fitting was obtained using 4 fixed gaussians at 2850, 2870, 2920 (CH<sub>2</sub>) and 2960 (CH<sub>3</sub>) cm<sup>-1</sup>. Standard deviations are given by the covariance value (%) between the spectra and their fit, and calculated from the weighted sum squared residual (WSSR).

## TOF SIMS Mass Spectrometry

The Time-of-Flight mass spectrometry analysis was performed on the TOF-SIMS IV (IONTOF GmbH, Germany) at the Laboratory of Molecular and Structural Archaeology (LAMSA, CNRS – Sorbonne University, Paris, France). The primary ion source used for analysis was a liquid metal ion gun delivering a bismuth cluster pulsed ion beam (25 keV energy Bi<sub>3</sub><sup>+</sup> ions) hitting the surface with an incidence angle of 45°, with a low energy electron flood gun neutralising the surface between each analysis scan. The time-of-flight analyser is equipped with delayed extraction of secondary ions, which offers the possibility of coupling a high spatial resolution with a mass resolution of a few thousand (M/ΔM, full width at half maximum). The analyses were then made using this so-called “burst alignment with delayed extraction” (BA+DE) focusing mode. The beam diameter can be reduced down to 400 nm because the long primary ion pulses (~100 ns) are compensated by the delayed extraction (DE) of the secondary ions (full description given by Vanbellinghen *et al.*, 2015). The primary dose was 5.10<sup>12</sup> ions/cm<sup>2</sup>. Before the analysis, a 500 μm side square around the analysed areas was cleaned with a dose of 2 to 4.10<sup>14</sup> ions/cm<sup>2</sup> using 10 keV argon clusters of 2000 atoms emitted by a Gas Cluster Ion Beam (GCIB), which allows a gentle sputtering of the surface without damaging the underlying layers, to remove surface contamination. Raw data were acquired using SurfaceLab 6.7 software (IONTOF GmbH, Germany) and processed with SurfaceLab 7.0. A typical statistical error was applied using the quadratic sum of signal intensities.

## Elemental Analysis

The bulk H-isotope measurements for Aguas Zarcas and Mukundpura were performed on an Elementar VISION interfaced with an Elementar pyrocube. About 1 mg of IOM were loaded into silver capsules. Capsules were stored in an autosampler set at 80 °C, then dropped into a 1450 °C furnace made in glassy carbon, and flushed by pure He. The instrument reproducibility and bias were checked using the CH<sub>7</sub> polyethylene standard from IAEA. Measurements were made in replicates.



## NanoSIMS Mass Spectrometry

The Cameca NanoSIMS 50 (MNHN, Paris) was acquiring  $\delta D$  and  $d15N$  images of IOMs, in two sessions. Pressed samples onto clean indium foil were gold coated (final 20 nm thick). Secondary ions of  $H^-$  and  $D^-$  were collected to obtain  $\delta D$  images and  $^{16}O^-$ ,  $^{12}C^{2-}$ ,  $^{26}CN^-$ ,  $^{27}CN^-$  and  $^{32}S^-$  for  $\delta^{15}N$  images. To minimise topographic effects on IOM N/C measurements,  $^{26}CN^-/^{12}C^{2-}$  was the ion ratio measured (Thomen *et al.*, 2014). Prior to any analysis, a  $25 \times 25 \mu m^2$  pre-sputtering was applied, for a duration of 10 minutes and using a 300 pA primary current. Its role was to remove the sample coating, clean the surface and to reach a sputtering steady state. For H and N isotopes, the primary  $Cs^+$  beam (16 keV) was set at 14 pA and 2 pA. The resulting spatial resolution was 300 and 150 nm, for hydrogen and nitrogen respectively. Image collection was set  $256 \times 256$  pixel covering  $20 \times 20 \mu m^2$ , with a raster speed of 1ms/pix. Electron multipliers were used, with a dead time of 44 ns in multicollection mode. The resulting mass resolving power was set at 5000 (for H) and for N isotopes it was increased to 9000, to resolve interferences such as  $^{12}C^{15}N^-$  from  $^{13}C^{14}N^-$  and  $^{32}S^-$  from  $^{16}O^{2-}$ . The vacuum was consistently below  $5 \times 10^{-10}$  torr. All NanoSIMS data were processed with L'Image software (Larry Nittler, Carnegie Institution in Washington DC, USA). Isotopic ratio and the elemental ratios were corrected using calibration lines, by measuring known reference samples: terrestrial type 3 kerogen from Virginia and charcoal as well as the IOM of Orgueil meteorites (Remusat *et al.*, 2016).

Uncertainties are 1 sigma errors, combining counting statistics uncertainties on each measurement and uncertainties from the calibration lines. Isotopic ratios are expressed in delta units, following the relation:

$$\delta (\text{‰}) = (R_{\text{sple}}/R_{\text{std}} - 1) \times 1000$$

with  $R_{\text{sple}}$  being the sample isotopic ratio and  $R_{\text{std}}$  the ratio of a terrestrial standard; Standard Mean Ocean Water (SMOW:  $D/H = 155.76 \times 10^{-6}$ ) for H isotopes and Air for N ( $^{15}N/^{14}N = 3.67 \times 10^{-3}$ ).

## EPR Spectroscopy

The EPR spectra were recorded with a Bruker Eleksys E500 spectrometer operating at X-band (microwave frequency  $\approx 9.4$  GHz), equipped with an 4122SHQE resonator and an Oxford ESR900 helium flow cryostat for sample cooling. A modulation of the magnetic field at 100 kHz with a 0.1 mT amplitude was applied for lock-in detection of the EPR spectra. The applied microwave power was 64  $\mu W$ , low enough to avoid saturation. Samples masses were 12.0 mg and 10.5 mg for AZ and MK samples, respectively. The spectra were recorded with the samples under vacuum, with a residual pressure  $\leq 10^{-3}$  mbar. The intensities of the spectra were calculated from  $A \times (\Delta B)^2$  where  $A$  is the peak-to-peak height and  $\Delta B$  the peak-to-peak width of the EPR line.



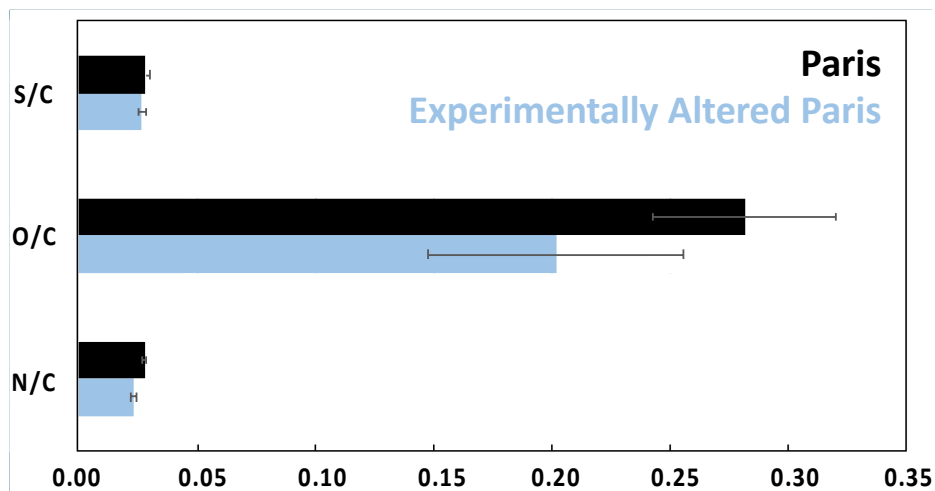


**Figure S-1** Evolution of elemental ratios. Comparison of S/C, O/C and N/C from NanoSIMS analysis of experimentally altered Paris H<sub>2</sub>O (blue) and Paris (black). For respectively Paris and the experimental residue, N/C =  $2.8 \pm 0.1$  and  $2.3 \pm 0.1$ , O/C =  $28.2 \pm 4.0$  and  $20.2 \pm 5.4$ , S/C =  $2.8 \pm 0.2$  and  $2.7 \pm 0.1$ .

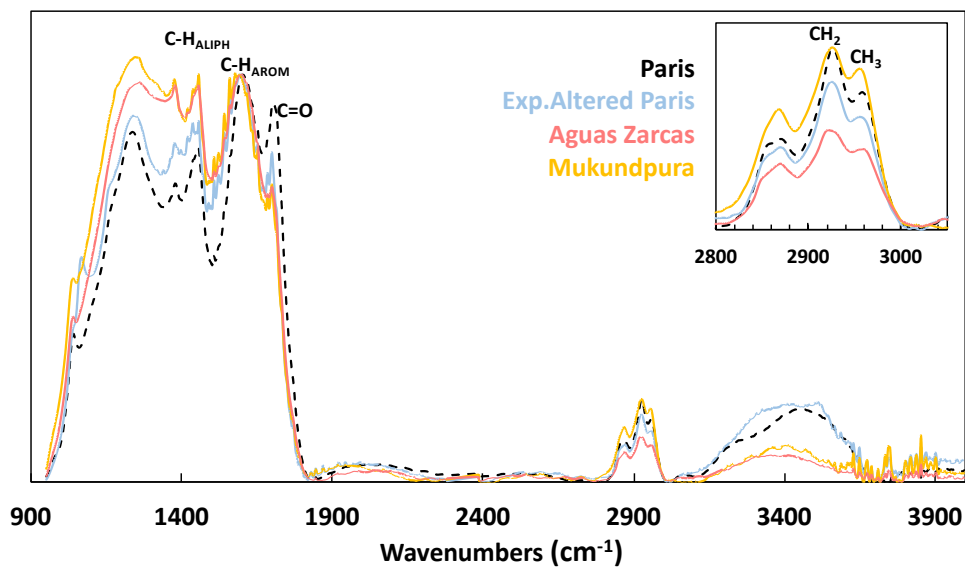


**Figure S-2** Infrared absorbance spectra of Paris (black), the experimentally altered Paris ('Altered Paris', blue), and altered CM2 Aguas Zarcas (pink) and Mukundpura (yellow), normalised to the C-H<sub>aromatic</sub> intensity. The black box is centred around the C-H stretch aliphatic area.

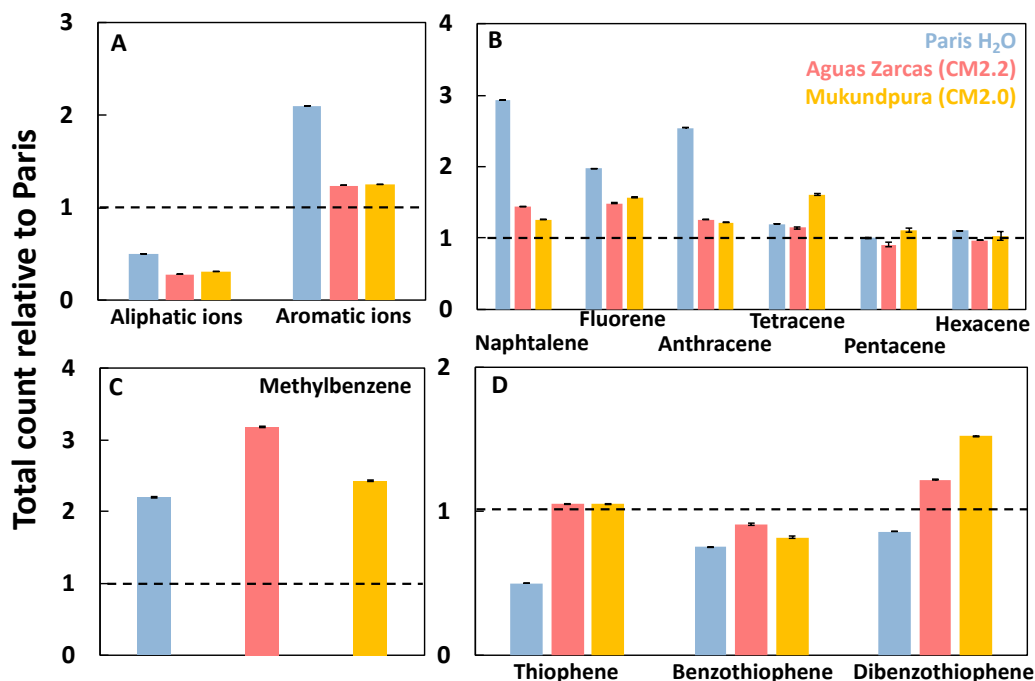


**Figure S-3** Comparison between experimentally altered IOM from Paris and recently recovered CM2 TOFF-SIMS data. **(a)** Relative Intensity of secondary aliphatic and aromatic ions, normalised to total carbon signal for PAHs, for experimentally altered Paris (blue), CM2.2 Aguas Zarcas (pink) and CM2.0 Mukundpura (yellow). **(b,c,d)** Idem for respectively PAHs, methylbenzene and thiophenic compounds. Mass and formula associated with detected fragments are reported on Table S-1 below.

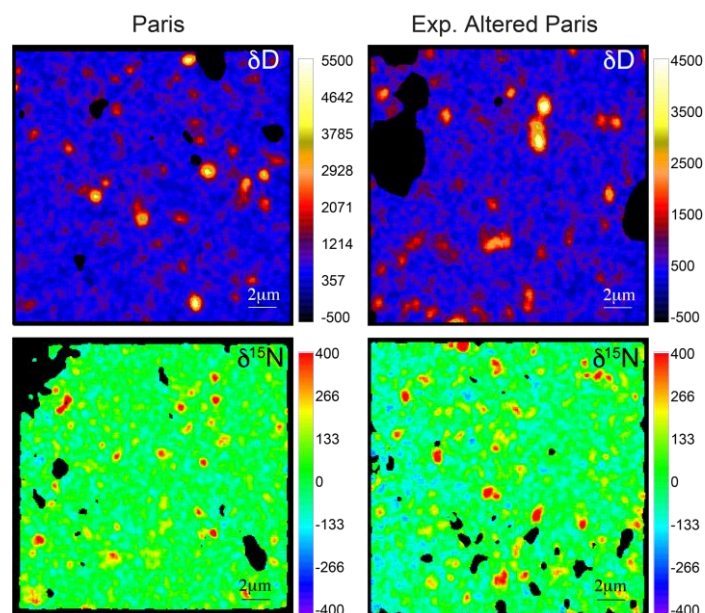


**Figure S-4** Nitrogen and hydrogen hotspot distribution. NanoSIMS images of H-isotope and N-isotope distribution in Paris (left) and experimentally altered Paris (right), each image covers a surface of  $20 \times 20 \mu\text{m}^2$ .

**Table S-1** Name, Mass and formula associated with detected carbon fragments in TOF SIMS.

<b>Molecular fragment</b>	<b>Formula</b>	<b>Mass</b>
methylbenzene	C <sub>7</sub> H <sub>8</sub> <sup>+</sup>	92.1
thiophene	C <sub>4</sub> H <sub>4</sub> S <sup>+</sup>	84.1
benzothiophene	C <sub>8</sub> H <sub>6</sub> S <sup>+</sup>	134.1
dibenzothiophene	C <sub>12</sub> H <sub>8</sub> S <sup>+</sup>	184.2
methylbenzene	C <sub>7</sub> H <sub>8</sub> <sup>+</sup>	92.1
<b>Aromatic ions</b>		
naphtalene	C <sub>10</sub> H <sub>8</sub> <sup>+</sup>	128.1
fluorene	C <sub>13</sub> H <sub>10</sub> <sup>+</sup>	166.1
anthracene	C <sub>14</sub> H <sub>10</sub> <sup>+</sup>	178.2
tetracene	C <sub>18</sub> H <sub>12</sub> <sup>+</sup>	228.3
perylene	C <sub>20</sub> H <sub>12</sub> <sup>+</sup>	252.2
pentacene	C <sub>22</sub> H <sub>14</sub> <sup>+</sup>	278.2
hexacene	C <sub>26</sub> H <sub>16</sub> <sup>+</sup>	328.5
coronene	C <sub>24</sub> H <sub>12</sub> <sup>+</sup>	300.2
heptacene	C <sub>30</sub> H <sub>10</sub> <sup>+</sup>	378.3
<b>Aliphatic ions</b>		
ethylene	C <sub>2</sub> H <sub>4</sub> <sup>+</sup>	28.0
ethane	C <sub>2</sub> H <sub>6</sub> <sup>+</sup>	30.0
cyclopropane	C <sub>3</sub> H <sub>6</sub> <sup>+</sup>	42.1
cyclobutenyl	C <sub>4</sub> H <sub>3</sub> <sup>+</sup>	51.1
isobutylene	C <sub>4</sub> H <sub>8</sub> <sup>+</sup>	56.0
pentane	C <sub>5</sub> H <sub>12</sub> <sup>+</sup>	72.1

## Supplementary Information References

- Belkhou, R., Stanescu, S., Swaraj, S., Besson, A., Ledoux, M., Hajlaoui, M., Dalle, D. (2015) HERMES: a soft X-ray beamline dedicated to X-ray microscopy. *Journal of Synchrotron Radiation* 22, 968–979. <https://doi.org/10.1107/S1600577515007778>
- Hitchcock, A.P. (2018) Influence of local environment on inner shell excitation spectra, studied by electron and X-ray spectroscopy and spectromicroscopy. *Zeitschrift für Physikalische Chemie* 232, 723–745. <https://doi.org/10.1515/zpch-2017-1061>
- Laurent, B., Maillard, J., Afonso, C., Danger, G., Giusti, P., Remusat, L. (2022) Diversity of chondritic organic matter probed by ultra-high resolution mass spectrometry. *Geochemical Perspectives Letters* 22, 31–35. <https://doi.org/10.7185/geochemlet.2224>
- Le Guillou, C., Bernard, S., De la Pena, F., Le Brech, Y. (2018) XANES-based quantification of carbon functional group concentrations. *Analytical Chemistry* 90, 8379–8386. <https://doi.org/10.1021/acs.analchem.8b00689>
- Remusat, L., Piani, L., Bernard, S. (2016) Thermal recalcitrance of the organic D-rich component of ordinary chondrites. *Earth and Planetary Science Letters* 435, 36–44. <https://doi.org/10.1016/j.epsl.2015.12.009>
- Swaraj, S., Belkhou, R., Stanescu, S., Rioult, M., Besson, A., Hitchcock, A.P. (2017) Performance of the HERMES beamline at the carbon K-edge. *Journal of Physics: Conference Series* 849, 012046.
- Thomen, A., Robert, F., Remusat, L. (2014) Determination of the nitrogen abundance in organic materials by NanoSIMS quantitative imaging. *Journal of Analytical Atomic Spectrometry* 29, 512–519. <https://doi.org/10.1039/C3JA50313E>
- Vanbellingen, Q. P., Elie, N., Eller, M. J., Della-Negra, S., Touboul, D., Brunelle, A. (2015) Time-of-flight secondary ion mass spectrometry imaging of biological samples with delayed extraction for high mass and high spatial resolutions. *Rapid Communications in Mass Spectrometry* 29, 1187–1195. <https://doi.org/10.1002/rcm.7210>
- Vinogradoff, V., Le Guillou, C., Bernard, S., Binet, L., Cartigny, P., Brearley, A.J., Remusat, L. (2017) Paris vs. Murchison: Impact of hydrothermal alteration on organic matter in CM chondrites. *Geochimica et Cosmochimica Acta* 212, 234–252. <https://doi.org/10.1016/j.gca.2017.06.009>
- Wang, J., Morin, C., Li, L., Scholl, A., Doran, A. (2009) Radiation damage in soft X-ray microscopy. *Journal of Electron Spectroscopy and Related Phenomena* 170, 25–36. <https://doi.org/10.1016/j.elspec.2008.01.002>
- Wojdyr, M. (2010) Fityk: a general-purpose peak fitting program. *Journal of Applied Crystallography* 43, 1126–1128. <https://doi.org/10.1107/S0021889810030499>

